IOP Publishing European Journal of Physics
Eur. J. Phys. **40** (2019) 045002 (27pp) https://doi.org/10.1088/1361-6404/ab1a7b

Development and characterization of a low-cost wind tunnel balance for aerodynamic drag measurements

Suthyvann Sor[1], Rafael Bardera[1], Adelaida García-Magariño[1], Juan Carlos Matías García[1] and Eduardo Donoso[2]

[1] Experimental Aerodynamics, Instituto Nacional de Técnica Aeroespacial (INTA), Torrejón de Ardoz, Madrid, Spain
[2] Escuela Técnica Superior de Ingeniería Aeronáutica y del Espacio (ETSIAE), Universidad Politécnica de Madrid (UPM), Madrid, Spain

E-mail: sors@inta.es

Received 8 January 2019, revised 8 April 2019
Accepted for publication 17 April 2019
Published 17 June 2019

Abstract

Drag force measurement is one of the most important data that can be obtained in wind tunnel tests. Drag force is directly related to the energy that a vehicle needs to move, and, therefore, to the fuel costs associated with it. For vehicles, drag forces are usually measured in wind tunnels. The typical instruments for drag measurement are the force balances, which are usually complex and expensive instruments. The aim of this investigation is to study the development of a low-cost in-house balance for drag measurements in a wind tunnel. Based on a commercial available load cell XFTC300 Series in combination with simple elements designed and manufactured at INTA, a balance capable of measuring the drag force to models in a considerably wide adjustable range has been developed and characterized. The balance has been calibrated and used in a wind tunnel. Tests were carried out on a truck model, a simplified frigate shape and an Ahmed Body to obtain the resistance coefficient and evaluate the operation of the balance.

Keywords: balance, load cell, balance calibration, drag coefficient, wind tunnel

(Some figures may appear in colour only in the online journal)

1. Introduction

In general, there are three main types of wind tunnel tests [1]. The first ones try to get punctual values of the flow variables such as pressure, temperature or velocity using different devices: pressure transducers, Pitot tubes, thermocouples or laser Doppler anemometry. Others tests focus on flow visualization using traditional smoke techniques or more advanced techniques such as particle image velocimetry. The last group of tunnel tests corresponds to the forces and moments measurements of a model using balances.

Force measurement in wind tunnel testing is one of the most important tests in the aeronautical and automotive industry. In particular, knowing the aerodynamic drag force is essential for the designers of any vehicle operating under the influence of atmospheric air during its displacement. The main reason is that resistance is directly related to the energy needed to move and is therefore associated with the operational costs that the vehicle will have during its operating life. In a world where the price of fuels are increasing from year to year, keeping attention and reducing drag force is a key point [2–4]. However, force measurements in wind tunnels usually require complex and expensive instruments.

A good overview of balances in general (types, components, static and dynamic calibration) and the problems associated to them can be found in fluid mechanics books such as Gonzalez *et al* [5] in its 7th chapter, entitled 'Components of a Wind Tunnel Balance'. In particular, they review the coupling effect between lift and drag measurements and non-stationary effects generated by the model vibrations during the tests. Another book that explains the general concepts of balances, in this case applicated to unmanned aerial vehicles (UAV's) is the book for engineering of Marques *et al* [6]. Its 5th chapter includes a good explanation about wind tunnel balance calibration and force measurements through an example of a UAV designed and tested at INTA's facilities (Spain), and, finally, a brief review of the acquisition and signal processing of the balance measurements are included. Another overview of balances can be found in the paper of Nan [7], which presents different methods for measuring drag force in wind tunnels, presenting the advantages and disadvantages of each method.

Investigations based on analyzing the strains sensors used to measure forces in balances (piezoresistive gauges, fiber optic gauges) [8], temperature sensors to compensate and correct the strain values measured [9] and load diagrams of multi-component balances [10] have been reported. In particular, Ulbrich [10] presented relationships between the loads applied during a balance calibration and the load components of a strain-gage balance, for which three different generic diagrams for direct-read balance, force balance and moment balance are presented, and a particular example of a combined load diagram starting from the manual calibration of the Ames MK-III-C commercial balance is shown.

The design of wind tunnel balances to measure model forces has been a common subject of investigations since the beginning [11–14] and is still an active field of research [15–20]. Examples of some earlier papers in this field are those of Merrian [11], Klein *et al* [12], Howie *et al* [13] and Flay *et al* [14]. The work of Merriam [11] described a simple aerodynamic balance used in a wind tunnel to measure lift, drag and balance moment by means of wires and displacement of lift and drag balance riders. The work of Klein *et al* [12] explained the re-design of the force measurement system present in the Galacit Wind Tunnel which was able to measure six force and moments components of a suspended model at different angles of attack and allowed to vary the yaw angle of the model. The improvement was the calibration and measurement process. The work of Howie *et al* [13] consisted of the design of a

balance suspension which had to work in a corrosive atmosphere (aluminum chloride). The measurement system was attached to a beam in which deformations were quantified using a strain-gauge bridge network. In addition, a sensitivity analysis of the ratio between input and output voltage was included. The work of Flay *et al* [14] consisted of a re-design of a wind tunnel test facility for yacht aerodynamic studies, including the balance system used in the University of Auckland to calibrate and measure aerodynamic forces and moments generated by wind over a yatch. Other related articles regarding the design of force balances are those of Smith *et al* [15], Vadassery *et al* [16], Sahoo *et al* [17], Nanda *et al* [18] and Kalaiarassan *et al* [19], which described the design process of force balance for impulsive aerodynamic forces type. Smith *et al* [15] used a combination of modeling and analysis techniques (the stress wave force measurement technique) to design a six components force balance for hypervelocity shock tunnel testing, while Vadassery *et al* [16] designed an external drag balance. Sahoo *et al* [17] described the design and development of an accelerometer-based thin flat balance system for typical flight configurations in impulsive facilities. Kalaiarassan *et al* [19] focused on the design aspects of one-dimensional force balance system for hypersonic vehicle. Finally, another recent work is the one of Tavakolpour-Saleh *et al* [20], which presented a novel multi-component strain-gauge external balance to measure drag, lift and pitching moment, with interference errors down to 2.01%.

Previous balances were designed to measure drag and lift forces, and in general, most of them were able to measure the six components. As discussed by Tavakolpour-Saleh *et al* [20], there are two types of balances to measure more than one component: multi-pieces external balances (which use single component load cells installed within a mechanical framework so that each cell is responsive to a specific direction) and multi-components load cells. The reason for the appearance of the first type is that multi-component load cells are rarely found in the market, and the consequence is that the calibration uncertainty estimation is an arduous task because of the interference errors [21]. However, for certain applications, such as the automotive industry, the most important force to measure is the drag force [2–4]. If only one component is needed, the force-balance cost can be reduced considerable. Some previous attempt to present the design process followed to get a low-cost balance for academic or basic research purposesis the design of a low-cost two component wind tunnel balance of Martin Morris and Scott Post [22]. They use two load cells that were able to measure the lift and drag in airplanes or ground vehicles models in an academic wind tunnel where the angle of attack of the model could be changed by means of a linear actuator. Another investigation for educational wind balance is a flexible rod designed by Raush *et al* [23]. However, little information is available of the design process of one-component force balance for wind-tunnel testing.

In this context, the aim of this paper is to describe the design, manufacture and assembly process carried out to get a low-cost balance for aerodynamic drag measurement in a wind tunnel. The goal was to achieve this using a miniature load cell XFTC300 Series combined with simple and reasonable cost elements such as steel bars, levers and bearings. First, the design concept evolution and the final detailed design are presented. Then the manufacturing process, the assembly and other components of the balance are described. Afterward, the calibration process of the balance will be explained. Finally, a series of results of aerodynamic drag of a scaled truck and a simplified frigate shape (SFS) obtained using the balance in a wind tunnel are presented.

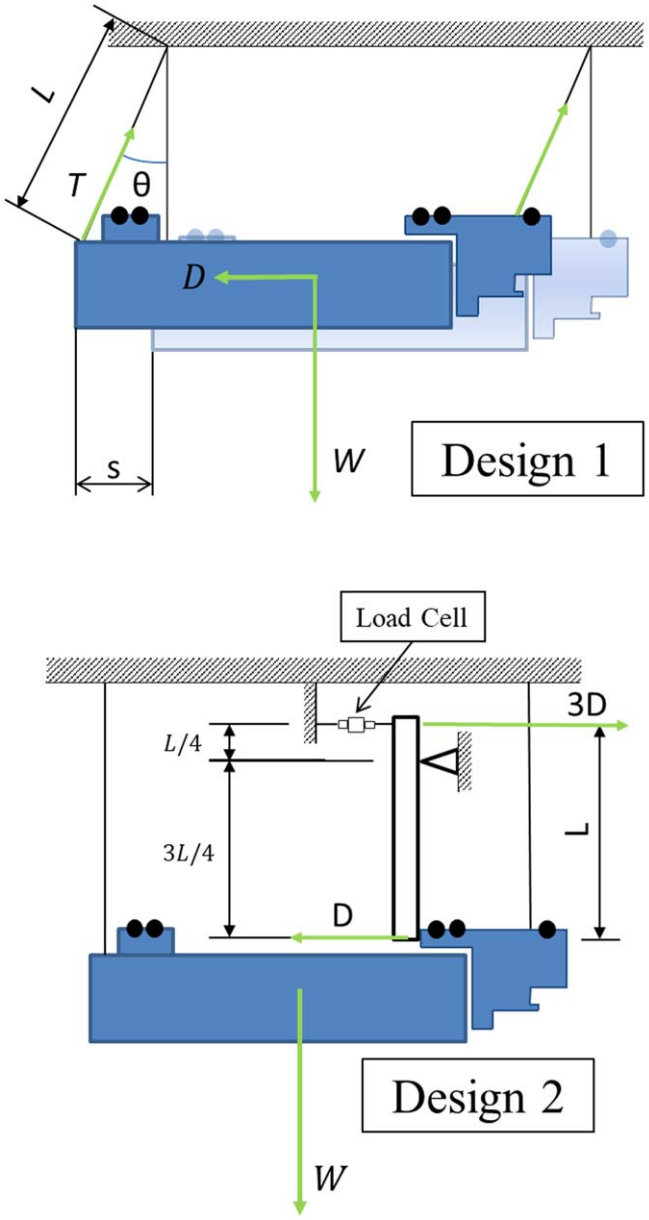

Figure 1. First and second conceptual designs.

2. Balance design, manufacture and assembly

2.1. Design concept evolution

The first simple solution studied was to suspend the model inverted by means of wires (design 1, figure 1). In their equilibrium position, the wires would be vertical. When the aerodynamic force acts on the model, the device would work like a pendulum. Then, the displacement of

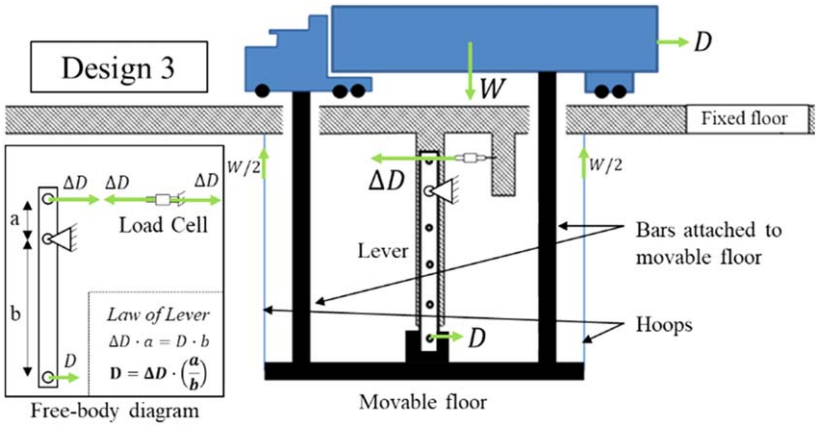

Figure 2. Third conceptual design. ΔD represents the drag force amplified according to the fixed lever point selected.

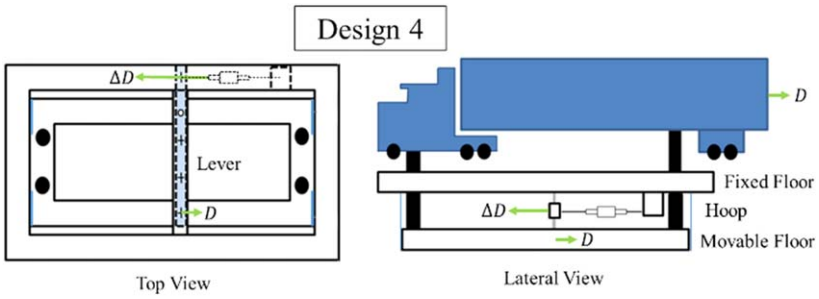

Figure 3. Final conceptual design.

the model (s) could be measured using a high-resolution camera. Finally, using the following equation system, it would be possible to calculate the drag (D):

$$\theta = \arcsin\left(\frac{s}{L}\right), \tag{1}$$

$$W = T\cos\theta, \tag{2}$$

$$D = T\sin\theta, \tag{3}$$

where W is the model weight, T the wire tension, θ the angle and D is the aerodynamic drag (figure 1, Design 1).

The main advantage of this first solution was that it was easy to assemble. However, as the incoming flow in the wind tunnel is not completely stable, oscillation would appear and would make it difficult to register the exact position of the model and determine the angle θ.

For a second alternative, a load cell was included in the design avoiding the need for a camera (design 2, figure 1). This cell contains a Wheatstone bridge which changes its electrical resistance when is deformed by tension or compression. The voltage drop in the load cell can be measured and translated into force by calibration. In addition, in order to extend the range of force measurements, a solution was thought by means of the Roman lever mechanism. In short, the second idea showed in figure 1 (Design 2) was a similar design to the first by adding the load cell. This design remained simple but improved its accuracy.

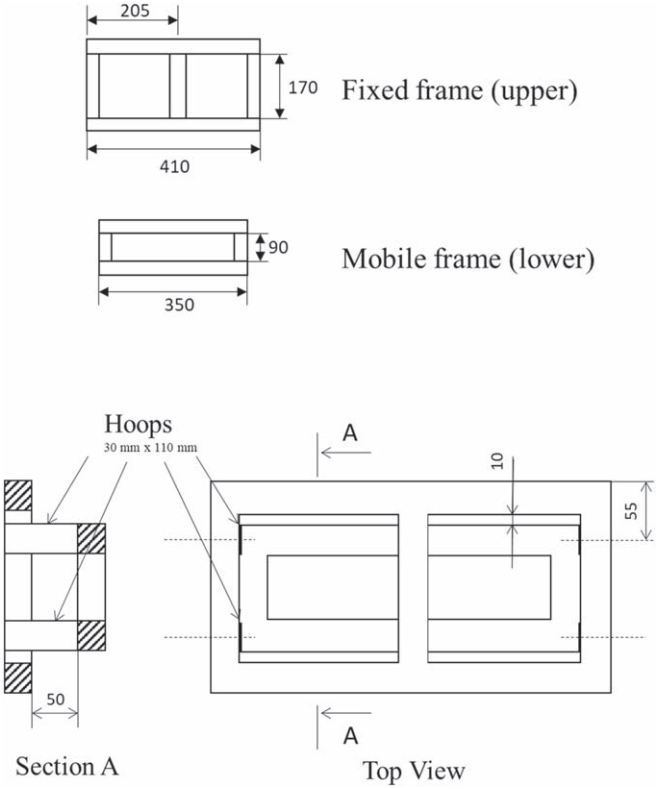

Figure 4. Frames and straps dimensions and attachment.

However, the absence of a floor could significantly affect the measurement of aerodynamic drag for land vehicles.

The third design analyzed is shown in figure 2. It was inspired by balances used in the automotive sector [24]. A movable floor is connected to a fixed floor by means of hoops. These hoops allow to support the weight of the model (traction) but no prevent the displacement in the direction of the aerodynamic drag (bending). A lever was again placed between the floors to multiply the force. In addition, the possibility of exchanging the fixed point of the lever to modify the multiplication ratio of the forces would be also implemented.

In order to avoid possible bar bending and to make the balance smaller, a last preliminary design was proposed (figure 3). To achieve this, it was decided to arrange the lever horizontally. This reduces the bars and straps length, making the design more compact, robust and handy.

2.2. Detailed design

The detailed design takes into account the wind tunnel test section size, the model dimensions and its weight. The final conceptual design consists of a main structure made up of two frames: a fixed frame (upper) attached to the wind tunnel test chamber and a mobile frame (lower) attached to the model by four bars. All the frames were made up of four welded 30 mm $\times$ 30 mm $\times$ 2 mm square section steel thin-walled tubes. The central tube of the upper frame serves as an anchorage point for the fixed point of the lever and provides additional rigidity to the structure.

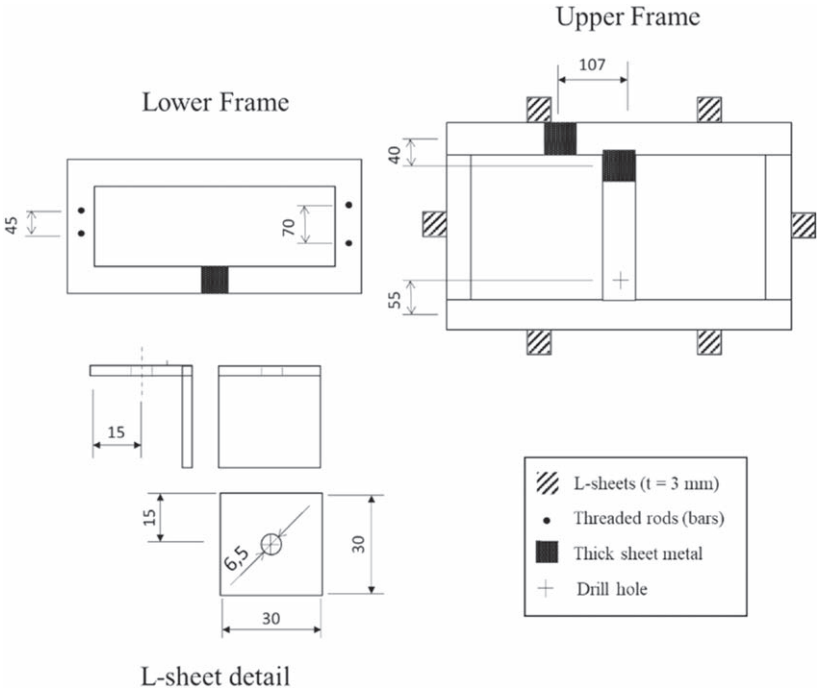

Figure 5. Upper and lower frames details.

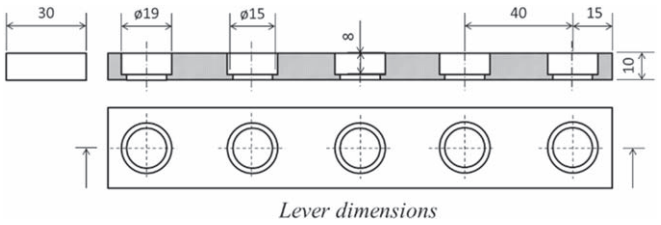

Figure 6. Lever design and dimensions.

Both frames are connected by four hoops (30 mm × 110 mm) that allow relative movement of the two frames (figure 4). A hood is a hardened metal band of high strength that allows movement only in their normal direction (the union of the hoops to the frames is M6 screwed, fixed with washers and nuts in the upper frame and threaded into the lower frame).

M10 threaded rods (bars) that connect the model to the lower frame are welded to the lower frame. Also, three 10 mm thick sheet metal are welded in order to join the lever with its three connection points (figure 5). Six L-sheets lugs welded to the upper frame are added for subsequent attachment to the floor of the balance. Finally, a drill hole in the central crossbar of the upper frame provides easy access to the connection point with the lower frame during the assembly.

A three-part mechanism, composed of a lever and two forks, is designed to translate the one-dimensional displacement of the model into force on the load cell.

The main part of the mechanism is the lever shown in figure 6. The external holes are used for the joining between the lower frame and upper frame through the load cell. The other three holes are used for the connection of the fixed point of the lever to the upper frame.

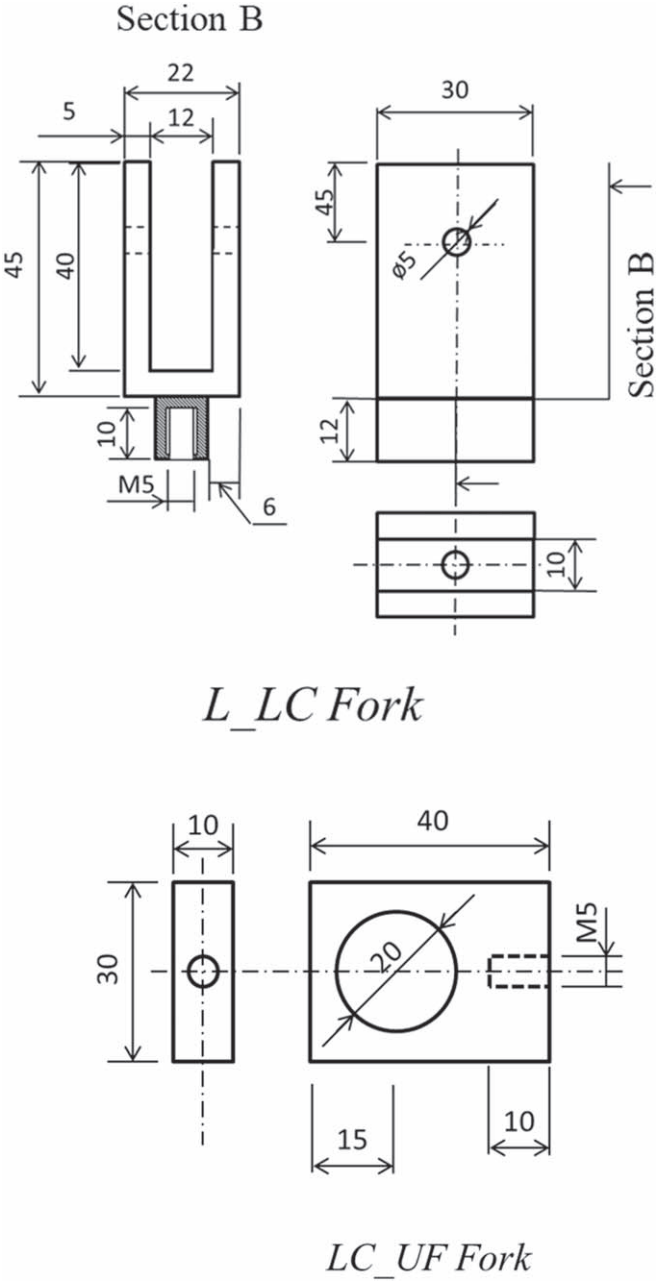

Figure 7. Lever and forks design and dimensions.

Changing it, it is possible to choose between three different power relations. The holes are the same size as the bearings that must be tightened in order to avoid the need for any other device such as elastic rings.

The lever is joined to the upper frame using two forks (figure 7). One transmits the force from the lever to the load cell threated into the M5 threaded hole (L_LC Fork). The

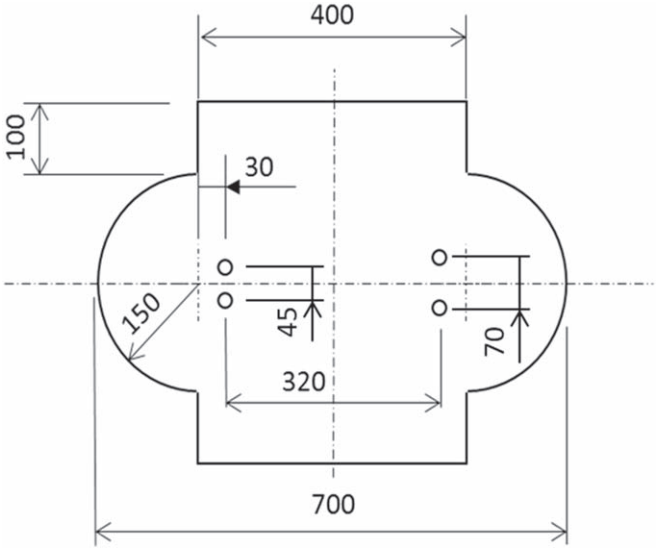

Figure 8. Floor dimensions of the balance.

connection between the lever and the fork allow rotation (so as not to transmit moments) and can be performed using an M5 screw fixed with a nut and several washers to prevent friction between the lever and the fork. The screw has to be tightened inside the bearing to prevent play during the measurement process.

The other fork (LC_UF Fork) connects the load cell with the upper frame (fixed). This connection also allow rotation to avoid torque transmission. To screw the piece to the upper frame and to ensure that it is at the desired height, a bearing was placed.

The XFC300 load cell has a working range between 2 and 50 N and can work under a temperature range between −20 and 100 C. Its thread is counter-locked to allow both sides to be tightened or loosened simultaneously to M5 threads of both forks.

All the structure is hidden under a floor (figure 8) which represents the floor of the model tested and its boundary condition. The floor is designed to be as large as possible, limited by the size of the tunnel test chamber used. The floor also has four drilled holes of 25 mm diameter to allow the passage of the threaded rods that will hold the model and must be joined to the lower frame.

Finally, to avoid interference of the airflow with the balance structure described above, it was necessary to design a fairing. The fairing was a prism with a section similar to an aircraft profile made of an aluminum sheet that is closed at the outlet edge with a riveted joint. Its height was 150 mm and is closed at the bottom by a wooden plank. It was joined to the floor by means of wooden stumps bolted to both the floor and the fairing.

2.3. Manufacturing

The entire manufacturing process, as well as the design, was carried out in the facilities of the Instituto Nacional de Técnica Aeroespacial 'Esteban Terradas', in Torrejón de Ardoz, Madrid. The manufacturing started with the two frames which were assembled by arc welding from steel tube 30 mm × 30 mm × 2 mm. The next step was to cut the threaded rods that were welded to the lower frame. The steel sheets for the bolted joints were then cut and the lugs

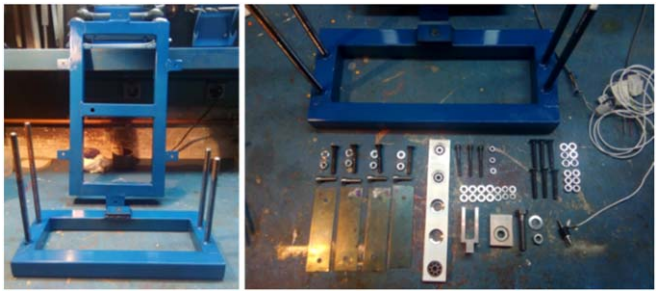

Figure 9. Upper and lower frames (left). Components ready for the assembly (right).

were manufactured and welded to the frames. The frames were finally drilled into the central crossbar and the welded locks. A coat of paint was given to protect frames from corrosion, as well as for aesthetic reasons.

The process continued with the manufacture of the three parts of the power transmission mechanism. All three, the lever and the two forks, were made of aluminum using a horizontal milling machine and a lathe, with precision to the tenth of a millimeter. The screw for the joint of the LC_UF fork with the upper frame was also manufactured. Once the parts had been manufactured, commercial ball bearings were added. The next step was to cut the four hoops (110 mm long $\times$ 30 mm width), and drill them. At this point, with all the components ready, the mechanism was assembled on the structure.

2.4. Assembly

The balance assembly (figure 9) begins with the union of the lever and the L_LC fork. Secondly, the fixed point of the lever is bolted to the upper frame, leaving 25 mm from the center of the lever to the face of the upper frame. The fixed point of the level selected for this assembly was the one with a $1/3$ ratio. That means that if the model makes a 10 N force (expected force for a 1:60 scaled truck), the load cell receives 30 N. The assembly continues by threading the load cell into the fork that connects it to the lever and once it is done, the LC_UF fork is threaded onto the other side. This fork is connected with the upper frame using a machined screw with a nut, washers and a bushing to ensure that the relative height is maintained and all the mechanism is in a horizontal plane.

The next step was to connect the frames through the hoops (figure 10), screwing them first to the upper frame using screws and nuts and then to the lower frame with lag bolts. Finally, the lever and the lower frame are screwed on.

For the balance floor, a 16 mm thick chipboard is used. It was cut with a wood panel saw and the leading edge was rounded off with a file. The necessary holes for the threaded rods and lugs were drilled. All holes were countersunk to keep the floor surface smooth. Finally, all the mechanism assembled was connected to the floor with screws and nuts.

To conclude the manufacturing process, a fairing was built using 1 mm thick aluminum sheet. It was shaped into a symmetric aerodynamic profile and large enough to surround and cover the core of the balance. The last hole was drilled in the fairing to allow the load cell wire to pass through. To attach the fairing, four wooden stumps were placed under the wooden floor of the balance. Thus, the sheet metal could be screwed to the rest of the assembly. The final exterior appearance of the balance is shown in figure 11.

Figure 10. Frames, straps and transmission power mechanism assembled (left). Balance core and wood flooring joined (right).

Figure 11. Balance assembled.

2.5. Others components of the balance

Once the mechanical part has been built, the electrical part must be designed to take measurements. The electrical assembly is summarized in figure 12.

The load cell XFTC300 Series used requires a DC supply voltage regulated between 1 and 10 V. An adjustable power supply model Transfer Multisort Elecktronik (TEM) MANSON EP-613 is used for this purpose. The output signal of the load cell indirectly provides the desired force measurement in another voltage. A multimeter Fluke MetraHIT 16 is used for this purpose.

3. Balance calibration

All instruments must be calibrated to reduce as far as possible systematic errors in the measured values and to check the equipment before starting to work with it. In this section, the balance calibration process is going to be described. Calibration was performed using an alignment laser, an inclinometer, a small crane with a pulley to hang the calibrated weights, a nylon thread, a DC power supply, a multimeter, and a hook to hang the eight weights (table 1). The following table shows the list of weights used in calibration.

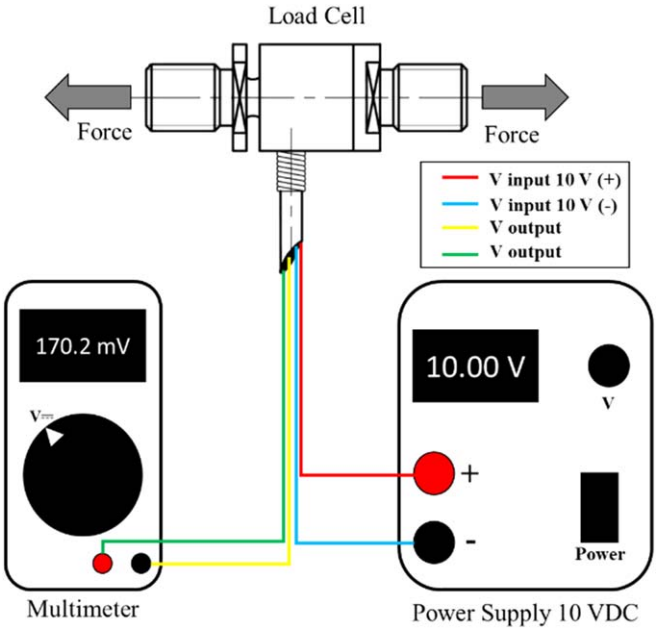

Figure 12. Electrical assembly for the load cell.

Table 1. List of weights used in calibration.

Number	Mass (kg)	Weight (N)
1	0.127	1.245
2	0.127	1.245
3	0.127	1.245
4	0.127	1.245
5	0.635	6.227
6	0.992	9.728
7	2.997	29.389
8	2.996	29.379
Hook	0.082	0.804

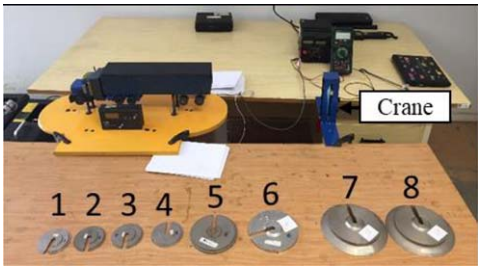

The crane was designed and built specifically for this calibration (figure 13). It was made from steel plates of 1 mm thickness. A guide was milled in it in order to move the pulley up and down and adjust the desired position. All the parts were joined by arc welding.

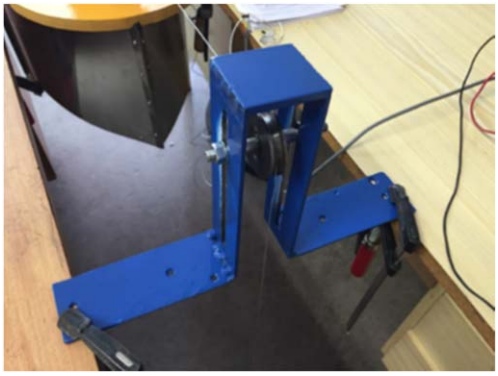

Figure 13. Crane manufactured for the calibration process.

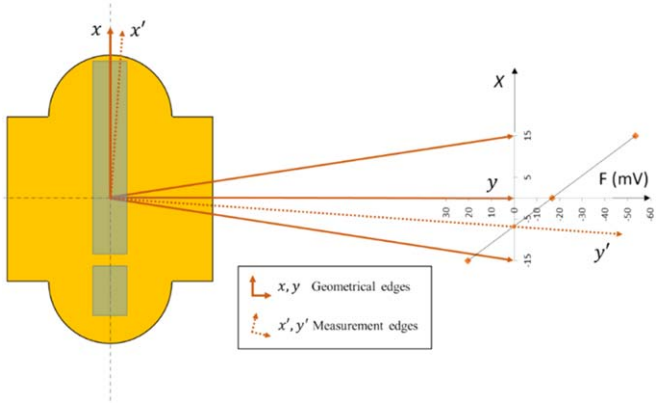

Figure 14. Geometrical and measurement edges of the balance. Interpolation process.

3.1. Directional calibration: main axes of the balance

The goal of the first stage of the calibration process is to determine the deviation of the measurement direction from the geometrical edges of the balance to the real measurement edges. The balance under study is a one-dimensional force measurement device and since force is a vector, its direction is relevant. Deviation in the vector is not desired and can be caused by manufacturing errors or lack of precision in the methods used. Its existence is inevitable but it should be small enough not to affect the proper operation of the instrument. The determination is vital to know the magnitude of the systematic errors in measurements.

The way to find the main axes of the balance consists of loading the balance with weights and angles close to the perpendicular direction to the load to measure (e.g. loading with lateral force, in the present case of drag measurement). Thus, the aim is to find the direction in which the balance always provides a zero signal if a force is applied. To achieve this, for each test the process was as follows (figure 14).

1. Draw the designed geometrical measuring direction (x).
2. Draw the perpendicular direction (y).

Table 2. Angle of deviation between geometrical and measurement edges of the balance.

Test	Angle $\beta(^\circ)$
1	−4.26
2	−4.21
3	−4.09
4	−4.13
Average	**−4.17**
σ	**0.08**

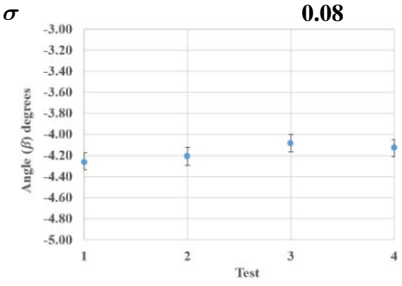

3. Take measurements by loading weights around the perpendicular direction drawn. Three measurements were taken 92.8 cm from the point of force application. The first just at the perpendicular point and then another two; one 15 cm to one side and another 15 cm to the other. The weights used was 7 and 8 to amplify the measurements.
4. Analysis of results. The three measurements are represented against their X position. With a simple interpolation, it is possible to obtain the point where the force measured is zero. This point defines the y'-axis of the measurement edges system.

This process was repeated four times, obtaining the results shown in table 2.

The vertical plane was obtained by the same procedure and the deviation was zero. That means that, in this case, the maximum measured point was obtained pulling with weights according to the horizontal direction ($\alpha = 0^\circ$).

3.2. Module calibration using calibrated weights

For the module calibration, weights were hung according to the horizontal plane by adjusting the height of the pulley (figure 15). The force was applied through a nylon wire attached to a pin in the model (trailer). In this way, the force is applied from the center of the model and does not rub against the model or the balance.

It is important to remark that the module calibration was done according to the geometric axes of the balance and not according to the measurement edges. This is because when the balance is placed in the tunnel, it will be positioned according to the geometric axes. The only consequence of this is that all the force results obtained must be divided by the cosine of the angle obtained from the directional calibration ($\beta = -4.17^\circ$).

To perform the module calibration, four up and down tests were carried out, covering a total of 14 load states each one. The load states cover the linear range of the load cell used, from a load of 2 N (minimum sensitivity) to just over 50 N. In addition, more cases were concentrated in the range where the balance is expected to operate, i.e. around 10 N on the model (30 N on the load cell due to the amplification achieved by the lever in the design).

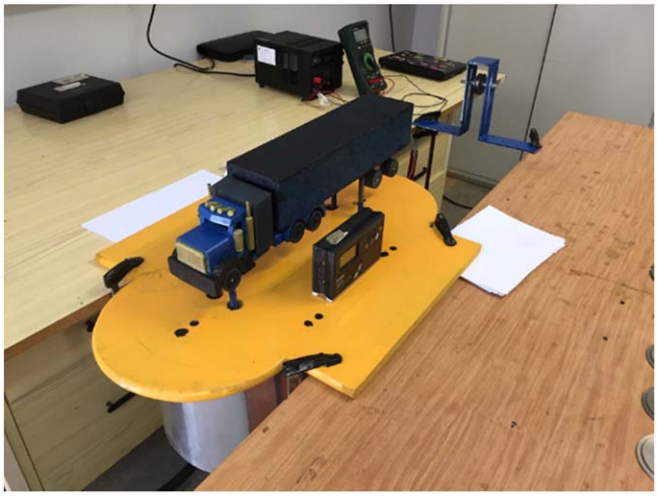

Figure 15. Performing module calibration.

Table 3. Results of test 1 module calibration.

Test	Weights	Force (N) applied (F)	Force (N) Load cell (3 F)	Upward output (mV)	Downward output (mV)	Average (mV)
1	H	0.80	2.41	169.6	167.0	168.3
2	H + 1	2.05	6.15	165.1	161.5	163.3
3	H + 1 + 2	3.29	9.88	158.8	154.9	156.9
4	H + 1 + 2 + 3	4.54	13.62	152.8	149.6	151.2
5	H + 1 + 2 + 3 + 4	5.79	17.36	147.3	144.4	145.8
6	H + 5	7.03	21.09	141.3	137.8	139.5
7	H + 1 + 5	8.28	24.83	134.3	130.9	132.6
8	H + 1 + 2 + 5	9.52	28.57	129.1	126.1	127.6
9	H + 6	10.53	31.59	124.7	122.8	123.8
10	H + 1 + 2 + 3 + 5	10.77	32.30	123.4	120.6	122.0
11	H + 1 + 6	11.78	35.33	118.4	116.4	117.4
12	H + 1 + 2 + 3 + 4 + 5	12.01	36.04	117.2	115.2	116.2
13	H + 1 + 2 + 6	13.02	39.07	112.1	107.7	109.9
14	H + 5 + 6	16.76	50.28	92.3	92.4	92.4

The results of the first of four tests are contained in table 3. This table shows the weights and forces applied during the test 1 of module calibration. The force applied in the load cell (3 F) is obtained by multiplying by a factor 3 selected during the assembly (law of lever) the force applied to the balance (F). The following columns show the readings of the output voltage of the load cell during the up and down tests. The last column shows

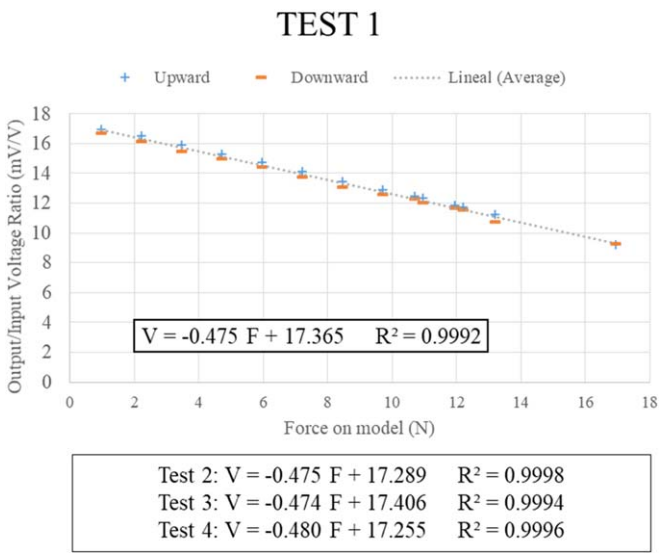

Figure 16. Load cell voltage ratio ($V_{ratio} = V_{out}/V_{in}$) of upward and downward cycles against the force applied to the model (F) during the four test. Calibration lines resultants of each test.

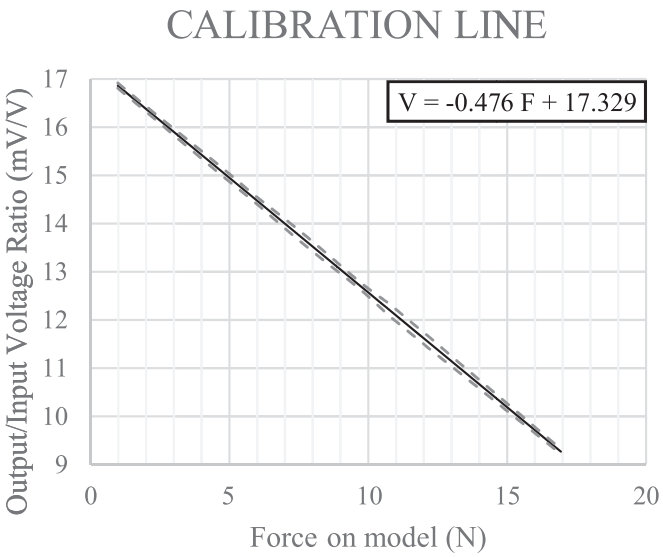

Figure 17. Calibration equation of the balance. Discontinuous bars above and below the straight line show the standard deviation of the measurements.

the average of both tests. An input voltage of $V_{in} = 10$ V has been always used for all tests.

The four experiments were carried out at different times of the day in order to perform them under different temperatures. The following graphs (figure 16) show the voltage ratio between output and input (mV/V) of the load cell against the force applied to the model

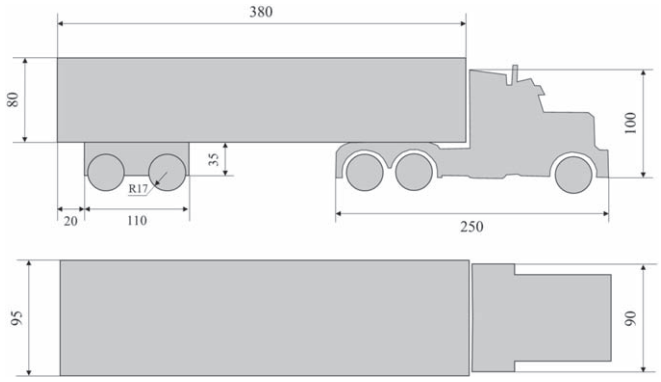

Figure 18. Main dimensions of the truck model (mm).

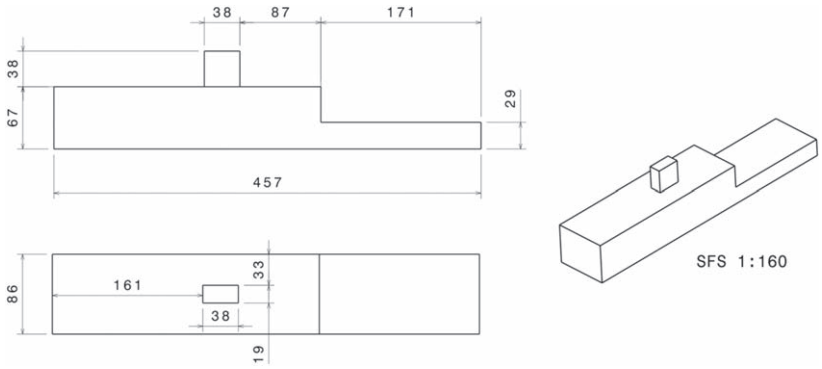

Figure 19. Dimensions of the simplified frigate model (SFS) 1:60th scaled.

during the four tests performed. Upward, downward cycles of each test are presented. Linear adjustment to the average points between both cycles in each test has been made to obtain their respective calibration equation.

The final calibration equation (figure 17) of the balance can be obtained making an average of all previous tests:

$$V_{\text{ratio}} = \frac{V_{\text{out}}}{V_{\text{in}}} = -0.476\,\text{F} + \epsilon_0. \tag{4}$$

Which equation can be easily reordered to obtain the drag force during the tests from the output voltage of the cell. The voltage ratio measured at the resting position of the balance $\epsilon_0 = V_{\text{resting}}/V_{\text{in}}$ (mV/V) is highly dependent on the temperature and must be quantified in each test:

$$F = D = \frac{V_{\text{ratio}} - \epsilon_0}{-0.476}. \tag{5}$$

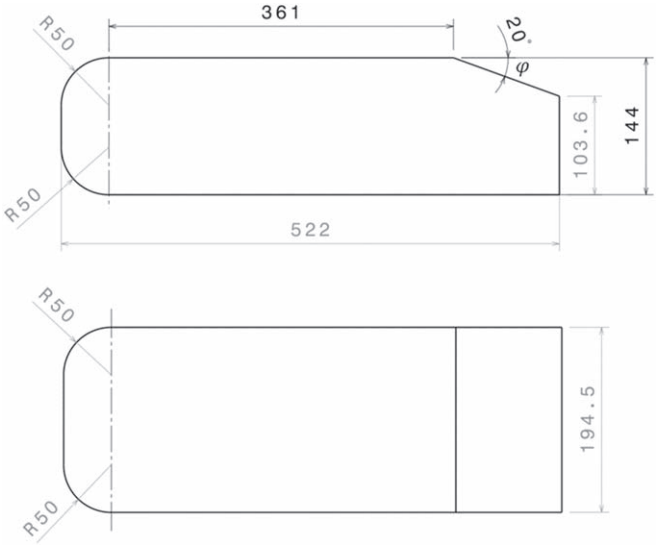

Figure 20. Dimensions of 1:2 scaled Ahmed Body tested.

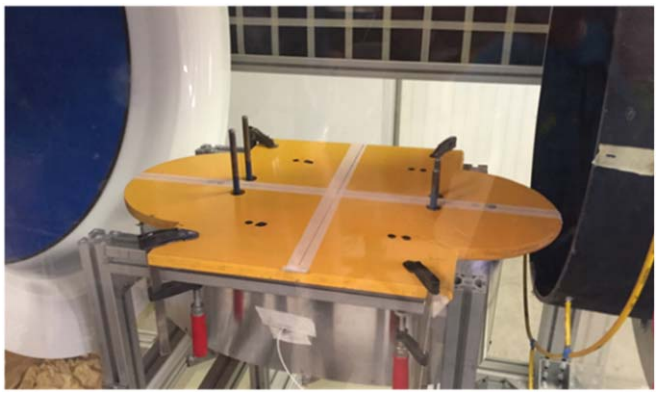

Figure 21. Balance placed in the test chamber of the wind tunnel.

All the results show that the load cell presents an initial state of compression load. This is because the higher load applied in traction, the lower is the output voltage of the load cell signal. In addition, a certain hysteresis was observed in the load cell since the output voltage was always lower during the load descent than in the ascent.

4. Balance testing

4.1. Models tested

The first scaled model used for testing the balance and obtaining its aerodynamic drag force was an American truck type. The model included the cab and its trailer on a $1/32$

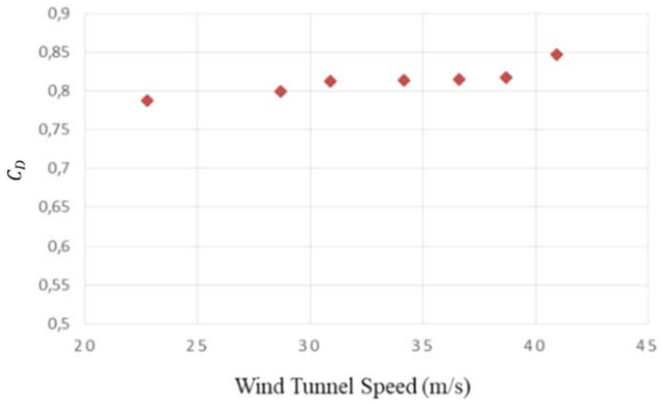

Figure 22. Drag coefficient of the threaded rods at different speeds (down).

scale. All dimensions of the model, including the cab and trailer are displayed in figure 18 below.

The other model tested was a simplified frigate ship (SFS) model [25, 26]. Its dimensions are showed in the following figure 19.

A last 'standard model' has been tested. Testing 'standard models' whose drag coefficients are known, is a normal practice to validate results using a new balance. For this purpose, one of the most used standard shapes is the Ahmed Body [27], which imitates a simple geometry of a car (figure 20). This model has been manufactured and tested using the balance.

4.2. Wind tunnel

The wind tunnel used for measuring aerodynamic drag using the balance was a Westenberg Engineering, WK 860060-E model. It is an open circuit wind tunnel with closed test chamber of 750 mm in width and 508 mm in height. The contraction ratio is 5.5. The 35 kW electrical engine allows reaching velocities up to 60 m s^{-1} at the test section. And two anti-turbulence screens to maintain the flow turbulence below 0.5%.

Figure 21 shows the wind tunnel test chamber during aerodynamic drag measurements of thread rods of the balance.

Taking into account the frontal surface of models tested and the wind tunnel chamber size, all tests were performed respecting the limit value of 15% of the total inlet section to avoid blockage effects [1].

4.3. Interference of threaded rods

To characterize the aerodynamic drag produced by the threaded rods, tests at different wind tunnel speeds (from zero to 41 m s^{-1}) were carried out (figure 22). The drag force of each test was obtained using the resultant expression from the module calibration tests:

$$D = \frac{V_{\text{ratio}} - \epsilon_0}{-0.476} - D_0, \tag{6}$$

where $D_0 = (V_{\text{ratio0}} - \epsilon_0)/(-0.476)$ is the force measured when the wind tunnel is switched off (0 m s^{-1}). Thus, average drag coefficient of the four rods obtained was $C_{D\ \text{rods}} = 0.846$, using the following expression:

Table 4. Reference surfaces for calculating drag coefficient of each model tested.

Test	$S_{\text{rods wet}}$ (cm^2)	S (cm^2)
American truck	4	112
SFS frigate	18	70
Ahmed Body	14.5	280

$$C_D = \frac{D}{q_\infty S} = \frac{D}{\rho V^2 S_{\text{rods}}} = \frac{D}{\frac{1}{2}\frac{p}{RT} V^2 S_{\text{rods}}}, \tag{7}$$

where $S_{\text{rods}} = 34.7$ cm^2 is the reference surface where the dynamic pressure q_∞ has been expressed as a function of pressure (p), temperature (T), and velocity (V), variables which can be measured in the wind tunnel during the tests. In order to compare the coefficient value with the results of tests using the truck, the drag coefficient obtained using the same reference surface $S_{\text{truck}} = 112$ cm^2 is $C^*_{D\,\text{rods}} = 0.26$. It must be taken into account that when the model is held by the rods, a large proportion of the bars are hidden inside the model. This means that the interference of the rods in the drag coefficient will be much lower than the value obtained in this section and must be estimated in each case.

4.4. Drag coefficient results of models tested

Drag force measurement on three different models (American truck, SFS frigate and Ahmed Body) were carried out. All tests were made at 15 different velocities, between 0 and 40 m s^{-1}. In addition, up-and-down cycles were performed to minimize the hysteresis effect of the load cell.

The drag force on each test (D) was obtained directly from the voltage measured at the load cell (V_{out}), using the resultant expression from the module calibration. This expression is corrected by means of an average between the measure of no-load condition at the beginning:

$$D_{0\,\text{start}} = (V_{\text{ratio start}} - \epsilon_0 / - 0.476)$$

at the end:

$$D_{0\,\text{end}} = (V_{\text{ratio end}} - \epsilon_0 / - 0.476)$$

and through the interference of the thread rods:

$$D = \frac{V_{\text{ratio}} - \epsilon_0}{-0.476} - \frac{(D_{0\,\text{start}} + D_{0\,\text{end}})}{2} - q_\infty\, S_{\text{rods wet}}\, C_{D\,\text{rods}}, \tag{8}$$

where ϵ_0 is the load cell voltage ratio under no-load condition, q_∞ is the dynamic pressure in each test and $S_{\text{rods wet}}$ is the wet surface and under aerodynamics effects of the thread rods when the model is placed on the balance (table 4).

Finally, drag coefficient (C^*_D) can be obtained using the following expression

$$C^*_D = \frac{D}{q_\infty S} = \frac{D}{\frac{1}{2}\rho V^2 S} = \frac{D}{\frac{1}{2}\frac{p}{RT} V^2 S}, \tag{9}$$

where the dynamic pressure q_∞ has been expressed as a function of pressure (p), temperature (T), and velocity (V), variables which can be measured in the wind tunnel during the tests. S is the frontal surface of the model (table 4) and $R = 287.04$ J kg^{-1} K^{-1} is the constant of the air.

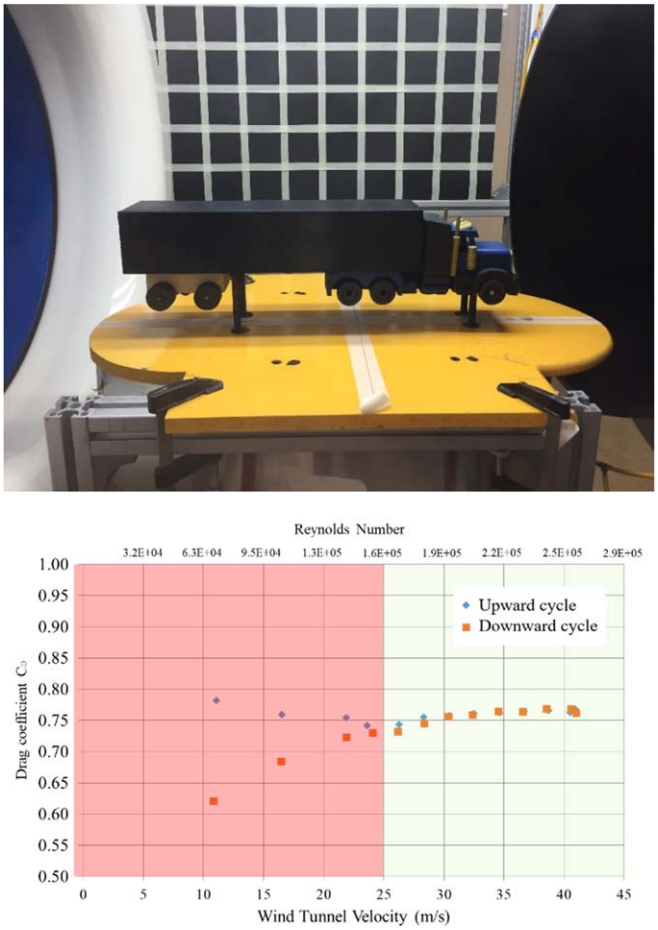

Figure 23. Truck model during the tests (up) and drag coefficient of the truck model against different wind tunnel velocities and Reynolds number (down).

Finally, making a last correction with the angle obtained by the directional calibration, the right drag coefficient of each model can be calculated as

$$C_D = \frac{C_D^*}{\cos(-4.17^\circ)}. \tag{10}$$

Figures 23–25 show photographs of models placed in the wind tunnel test chamber. Next to each photograph, plots with the drag coefficient obtained during the upward and downward cycles, against wind tunnel velocity (and Reynolds) are also presented. All data points have been obtained applying equations (8)–(10) from the voltage measured at the load cell (V_{out}) during the tests.

All measurements below 25 m s^{-1} must be discarded since the value of the coefficient is only constant above. This happens due to two reasons. The signal at this zone was too low and is greatly affected by electrical noise and minimal errors. In addition, the Reynolds number is not sufficiently above its critical value ($\sim 10^5$) up to reach 25 m s^{-1}.

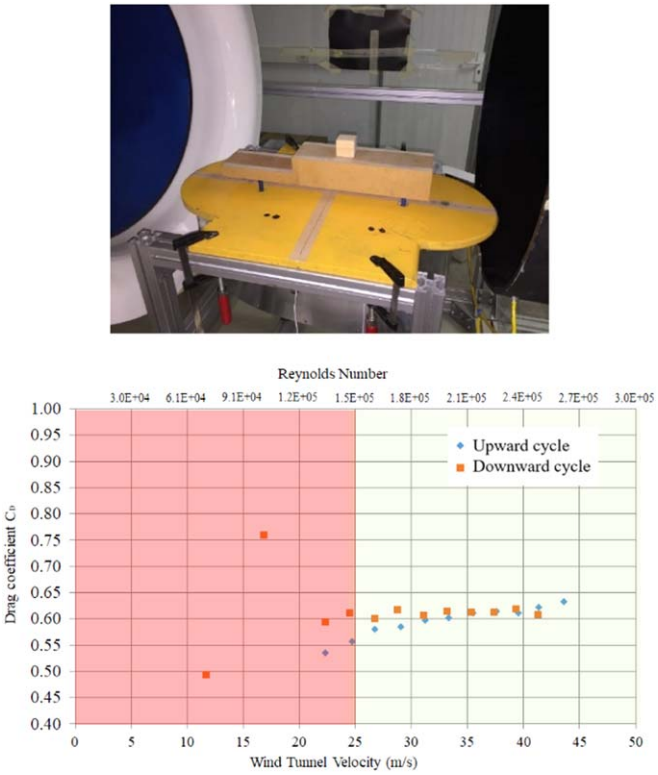

Figure 24. SFS frigate model during the tests (up) and drag coefficient of the SFS model at different wind tunnel velocities and Reynolds number (down).

Therefore, taking only the average of C_D values obtained above $25\,\mathrm{m\,s^{-1}}$, the drag coefficient obtained for the American truck model, the SFS and Ahmed Body using the balance designed are

$$C_{D_{\mathrm{Truck}}} = 0.76,$$

$$C_{D_{\mathrm{SFS}}} = 0.61,$$

$$C_{D_{\mathrm{AB}}} = 0.24.$$

The drag coefficients values obtained are in accordance with the expected result for a truck in clean configuration, i.e. without any flow control device to minimize the drag force ($\sim 0.7 - 0.8$) [28]. The Ahmed Body drag coefficient obtained is also in accordance with the results expected (~ 0.25) [27]. It means an absolute error of $\sim 4\%$.

4.5. Measurement uncertainty analysis

Drag coefficient is a function which depends on the drag D, density ρ, velocity V_∞ and surface S:

$$C_D = \frac{D}{\frac{1}{2}\rho V_\infty^2 S} = f(D,\ \rho,\ V_\infty,\ S). \tag{13}$$

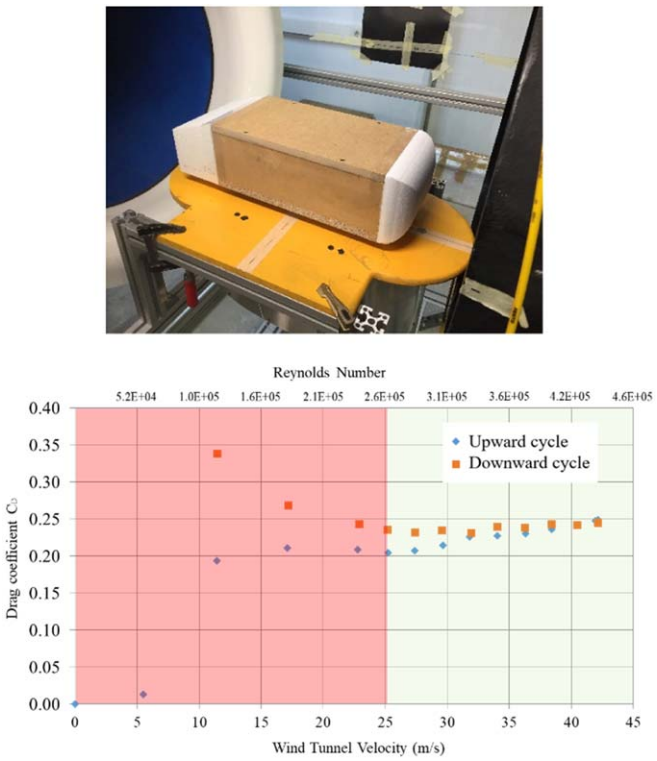

Figure 25. Ahmed body model during the tests (up) and drag coefficient of the Ahmed Body model at different wind tunnel velocities and Reynolds number (down).

The uncertainty value of the drag coefficient (u_{C_D}) can be obtained as the sum of partial derivatives of the previously mentioned variables:

$$u_{C_D}^2 = \left(\frac{\partial f}{\partial D}\right)^2 u_D^2 + \left(\frac{\partial f}{\partial \rho}\right)^2 u_\rho^2 + \left(\frac{\partial f}{\partial V_\infty}\right)^2 u_{V_\infty}^2 + \left(\frac{\partial f}{\partial S}\right)^2 u_S^2. \tag{14}$$

Considering all the uncertainty terms negligible except the one due to aerodynamic drag force (u_D):

$$u_{C_D}^2 \approx \left(\frac{\partial f}{\partial D}\right)^2 \cdot u_D^2 = \left(\frac{2}{\rho V_\infty^2 S}\right)^2 \cdot u_D^2 = \left(\frac{2D}{\rho V_\infty^2 S}\right)^2 \cdot \left(\frac{u_D}{D}\right)^2 = C_D^2 \cdot \left(\frac{u_D}{D}\right)^2. \tag{15}$$

The linear equation that relates the measured voltage (V) using the balance and the drag force (D) follows:

$$D = a + bV = f(V), \tag{16}$$

where $b = (1/-0.476)$ according to equation (5).Then, uncertainty value of the drag force (u_D) can be obtained as

$$u_D^2 = \left(\frac{\partial f}{\partial V}\right)^2 \cdot u_v^2 = b^2 \cdot u_v^2, \tag{17}$$

where u_v is the uncertainty value of the voltage:

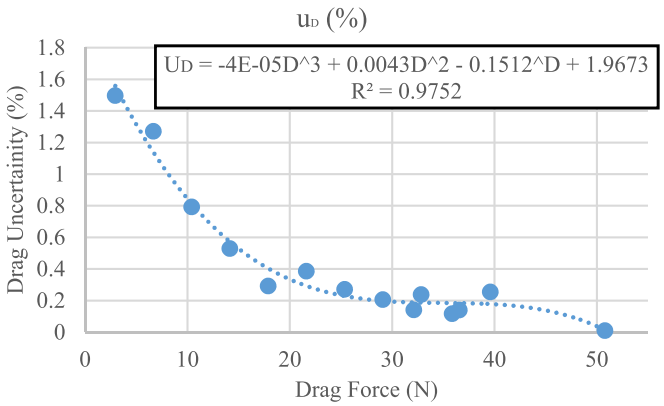

Figure 26. Polynomial adjustment of drag force uncertainty $u_D(\%)$.

Table 5. Results of 'Check Loads' tests.

Test	Weights (g)	Force applied (N)	Force measured (N)	True uncertainty (%)
1	127	1.25	1.07	13.8
2	381	3.74	3.65	2.4
3	571	5.60	5.59	0.1
4	762	7.48	7.46	0.3
5	953	9.35	9.39	0.4
6	1143	11.21	11.28	0.6
7	1397	13.7	13.72	0.1
8	1541	15.12	15.09	0.2
9	1794	17.6	17.53	0.4
10	1985	19.47	19.34	0.7
11	2112	20.72	20.44	1.3
12	2366	23.21	22.85	1.6
			AVG =	**1.8%**

$$u_v^2 = (u_v)_A^2 + (u_v)_B^2 = \left(\frac{\sigma_v}{\sqrt{n}}\right)^2 + (u_{\text{resol}}^2), \tag{18}$$

where σ_v is the typical deviation of the voltage measurements during calibration process, $n = 80$ is the number of measurements registered in each load state of that process (up and down, 4 tests $\times$ 10 measures) and $u_{\text{resol}} = 0.1 \times 10^{-3}$ V is the multimeter measurement resolution.

Figure 26 shows drag force uncertainty (u_D) as a function of drag measured using the balance through a third order polynomic adjustment to the points $u_D(\%) = f(D)$:

$$u_D(\%) = \frac{u_D}{D} \cdot 100. \tag{19}$$

Combining equation (15) and the adjusted equation for $u_D(\%) = f(D)$:

$$(u_{C_D})^2 \approx C_D^2 \cdot \left(\frac{u_D}{D}\right)^2 = C_D^2 \cdot \left(\frac{f(D) \cdot D/100}{D}\right)^2. \tag{20}$$

Drag coefficient uncertainty combined and expanded with 95% probability ($K = 2$) can be obtained:

$$U_{C_D} = K \cdot u_{C_D}. \tag{21}$$

Replacing now the values in equations (20) and (21) with those obtained during truck and SFS tests (only values over 25 m s^{-1}), the mean uncertainty value for drag coefficient for each case is

$$C_{D_{\text{truck}}} = 0.76 \pm 0.02 \text{ (2.5\% uncertainty)}, \tag{22}$$

$$C_{D_{\text{SFS}}} = 0.61 \pm 0.02 \text{(3.1\% uncertainty)}, \tag{23a}$$

$$C_{D_{\text{AB}}} = 0.24 \pm 0.01 \text{ (4\% uncertainty)}. \tag{23b}$$

Finally, twelve 'Check Loads', using different weights from those ones used during the calibration process, were used to obtain the standard deviation of errors between applied load and measured load (value using calibration line). A true uncertainty value in load measurement has been obtained (table 5).

5. Conclusions

In this paper, the design, manufacturing and assembly process of a hand-made balance to measure drag force in wind tunnel models has been described. It has only been necessary to use a reasonably low-cost load cell and some elements were manufactured using steel and aluminum. Afterwards, the processes of directional and module calibration have been explained. It has been demonstrated that it is essential to perform a correct calibration of the instrument in order to achieve the most accurate results possible. For example, the existence of misalignment in the force application (β) could have been a source of 2% error, if it had not been corrected by directional calibration.

From the module calibration and the tests it is clear that there is hysteresis in the instrument. This was observed during the calibration phase and during the tests performed in which the greatest response was in the downward cycle of the load states. However, all the results have been corrected to prevent errors from hysteresis.

In addition, the resting position of the instrument is highly dependent on temperature. Thus, the coordinate origin of the calibration line, or, in other words, the output value in mV in the no-load position (ϵ_0) is temperature-dependent. During all tests this value oscillated between 177 and 132 mV, and its change must be taken into account on each test using the balance. The best way to characterize the ϵ_0 value and minimise the hysteresis effect is to make an average between the no-load position before and after each test.

Tests made to a truck model show that the drag force obtained by the balance and the drag coefficient derived from that is in accordance with the expected. The same happened with the measurements made with the SFS and the Ahmed Body 'standard model' tested.

A final uncertainty analysis have been made in order to estimate the errors of the drag coefficient values achieved. Uncertainties around 2% in the load force measurement and between 2.5% and 4% in the drag coefficient estimation have been achieved with this low-cost balance thanks to the large number of measurements taken during calibration process.

A possible improvement of the balance designed and described in this article is in the data acquisition. Instead of taking manual readings of the output voltage, it would be desirable to incorporate an automatic data acquisition system at a given frequency. Another improvement for future work would be to use the basic design principles outlined here to manufacture a balance to measure more force and moment components (up to three forces and three moments).

To conclude, it has been shown that it is possible to build a wind tunnel balance to provide fairly accurate results. The design followed in this paper could be useful to anyone who wants to measure drag force in wind tunnel models, for academic or basic research studies.

Acknowledgments

This research has been supported by the Spanish INTA internal Project 'Termofluidodinámica'.

ORCID iDs

Rafael Bardera https://orcid.org/0000-0002-5157-9935
Juan Carlos Matías García https://orcid.org/0000-0001-6049-6421

References

[1] Barlow J, Rae W and Pope A 1999 *Low-speed Wind Tunnel Testing* (New York: Wiley)
[2] Roy S and Srinivasan P 2000 *External Flow Analysis of a Truck for Drag Reduction* (Flint: Kettering University) (https://doi.org/10.4271/2000-01-3500)
[3] Cresswell M G L and Hertz P B 1992 Aerodynamic drag implications of exterior truck mirrors *SAE Technical Paper Series* pp 29–34 No. 920202
[4] Wood R M and Bauer S X S 2003 Simple and Low-Cost Aerodynamic Drag Reduction Devices for Tractor-Trailer Trucks *SAE Technical Paper* 2003-01-3377 (https://doi.org/10.4271/2003-01-3377)
[5] Gonzalez M, Miguel Ezquerro J, Lapuerta V, Laveron A and Rodriguez J 2011 *Components of a Wind Tunnel Balance: Design and Calibration, Wind Tunnels and Experimental Fluid Dynamics Research* ed J C Lerner (Rijeka: InTech) (https://doi.org/10.5772/21095)
[6] Marques P and Da Ronch A 2017 *Advanced UAV Aerodynamics, Flight Stability and Control: Novel Concepts, Theory and Applications* (New York: Wiley) (https://doi.org/0.1002/9781118928691)
[7] Nan L 2013 The methods of drag force measurement in wind tunnels. faculty of engineering and sustainable development *Master's Thesis in Energy Systems* University of Gävle
[8] Webster J and Hazarian E 1999 Strain Measurement *The measurement, instrumentation, and sensor handbook* 1st edn (Boca Raton, FL: CRC Press) ch 22
[9] Vukovic D, Samardzic M and Vitic A 2008 Prototype of a stiff wind tunnel balance with semiconductor strain gauges and thermocompensation done by software *26th Int. Congress of the Aeronautical Sciences*
[10] Ulbrich N 2010 Combined load diagram for a wind tunnel strain-gage balance *27th AIAA Aerodynamics Measurement and Ground Testing Conf. (Chicago, Illinois)* Jacobs Technology Inc., Moffett Field, California 94035-1000 (https://doi.org/10.2514/6.2010-4203)
[11] Merriam K G 1936 Equipment for laboratory instruction in aerodynamics *J. Aeronaut. Sci.* **3** 353–5
[12] Klein A L 1942 A new two-parameter model suspension system for the galcit 10-Ft. Wind tunnel *J. Aeronaut. Sci.* **9** 302–8
[13] Howie R and Macmillan D 1972 A strain gauge balance suspension *J. Phys. E: Sci. Instrum.* **5** 851–3
[14] Flay R and Vuletich I 1995 Development of a wind tunnel test facility for yacht aerodynamic studies *J. Wind Eng. Ind. Aerodyn.* **58** 231–58

[15] Smith A, Mee D, Daniel W and Shimoda T 2001 Design, modelling and analysis of a six component force balance for hypervelocity wind tunnel testing *Comput. Struct.* **79** 1077–88
[16] Vadassery P, Joshi D, Rolim T and Lu F 2013 Design and testing of an external drag balance for a hypersonic shock tunnel *Measurement* **46** 2110–7
[17] Sahoo N, Mahapatra D, Jagadeesh G, Gopalakrishnan S and Reddy K 2007 Design and analysis of a flat accelerometer-based force balance system for shock tunnel testing *Measurement* **40** 93–106
[18] Nanda S, Kulkarni V and Sahoo N 2016 Design of artificial neuro-fuzzy based methodology for six component force balance *Procedia Eng.* **144** 528–36
[19] Kalaiarassan G, Krishan, Somanadh M, Thirumalai C and Senthil Kumar M 2018 One-dimension force balance system for hypersonic vehicle an experimental and fuzzy prediction approach *Mater. Today: Proc.* **5** 13547–55
[20] Tavakolpour-Saleh A, Setoodeh A and Gholamzadeh M 2016 A novel multi-component strain-gauge external balance for wind tunnel tests: simulation and experiment *Sensors Actuators* A **247** 172–86
[21] Reis M, Castro R and Mello O 2013 Calibration uncertainty estimation of a strain-gage external balance *Measurement* **46** 24–33
[22] Morris M and Post S 2010 *Force Balance Design for Educational Wind Tunnels. Conf. Paper* (Bradley University. American Society for Engineering Education)
[23] Raush G, Castilla R, Gamez-Montero P, Wojciechowski J and Codina E 2013 Flexible rod design for educational wind balance *Exp. Tech.* **40** 111–9
[24] Chowdhury H, Moria H, Ali A, Khan I, Alam F and Watkins S 2013 A study on aerodynamic drag of a semi-trailer truck *5th BSME Int. Conf. on Thermal Engineering. School of Aerospace, Mechanical and Manufacturing Engineering* (Melbourne, VIC 3083, Australia: RMIT University) (https://doi.org/10.1016/j.proeng.2013.03.108)
[25] Reddy K R, Toffoletto R and Jones K R W 2000 Numerical simulation of ship airwake *Comput. Fluids* **29** 451–65
[26] Syms G F 2008 Simulation of simplified-frigate airwakes using a lattice-Boltzmann method *J. Wind Eng. Ind. Aerodyn.* **96** 1197–206
[27] Ahmed S, Ramm G and Faltin G 1984 Some salient features of the time-averaged ground vehicle wake *SAE Technical Paper 840300* (https://doi.org/10.4271/840300)
[28] Scania E P 2019 Experimental methods in vehicle aerodynamics KTH Vehicle Aerodynamics, Fluid Mechanics (https://www.mech.kth.se/courses/5C1211/KTH_Scania1.pdf)